REDUCED-ORDER MODELLING OF MINERAL DUST DEPOSITION IN TURBOSHAFT ENGINE HOT SECTIONS

Matthew Ellis[1], Nicholas Bojdo[2], Antonio Filippone[3], Merren Jones[4], Alison Pawley[5]

University of Manchester (GBR) [1,2,3,4,5]

[1]matthew.ellis@manchester.ac.uk

ABSTRACT

Operating in brownout conditions is a hazardous yet often unavoidable consequence of using rotorcraft in dry, arid environments. Significant quantities of the lofted dust cloud can be ingested into the helicopters engines where they cause damage in both the main gas path and secondary air systems. Molten particle accumulation on nozzle guide vanes has the potential to restrict the core mass flow and cause the engine to surge. Predicting the conditions under which this happens is complicated by the many separation and sorting processes that occur in the preceding sections of the engine. This contribution demonstrates a reduced-order, probabilistic methodology that can be used in conjunction with in-field particle sampling to predict the extent of nozzle guide vane damage and assess the risk of engine surge when operating in a particular environment. The processing of the raw ingested dust in the compressor and particle separator system is shown to be significant in accurately predicting the extent of damage and suggests that taking particle samples from the bulk dust cloud is likely to provide under-estimations of the actual damage seen in the engine.

1. INTRODUCTION

1.1. Rotorcraft Brownout

Rotorcraft have a unique versatility in being able to operate to and from remote, challenging locations with unprepared landing sites such as arid deserts. A by-product of this adaptability is the exposure to harsh environments such as the production of *'brownout'* clouds as shown in Figure 1. This is the lofting of surface sediment by impingement of the rotor wake on the ground, producing a densely concentrated cloud of suspended particulates which can rapidly envelop the entire airframe when operating at low altitudes [1].

Figure 1: A Royal Air Force AW-101 'Merlin' Helicopter performing a landing manoeuvre in brownout conditions (Courtesy of MoD Defence Imagery).

The production of a brownout cloud is the result of two mechanisms; ground-wash and suspension. The high velocity downwash from the rotor causes a *'ground-wash'* which pushes larger particles ($d_p > 20\mu m$) radially outwards from the rotorcraft. The result of this is that these particles are not lofted for extended periods of time and therefore do not contribute significantly to the bulk concentration of the dust cloud. More significant in the determination of the cloud concentration is long term suspension of smaller particles which are strongly influenced by the vortices formed at the rotor blade tips [2]. Individual vortices are convected from the rotor tips towards the ground where they bundle and combine, producing a large, single vortex which causes significant quantities of relatively smaller ($d_p < 20\mu m$) ground sediment to be uplifted, where it can be maintained in suspension for long periods of time. It is for this reason that rotorcraft with high blade counts can have significantly worse brownout signatures compared to those with lower blade counts, despite producing a weaker downwash [2].

Brownout events result in dust cloud concentrations which regularly exceed those seen naturally, even during worst case scenarios. For example, the background concentration in a typical dusty environment is around 0.1 mg/m^3, potentially increasing to 10mg/m^3 during a dust storm. By contrast, the Bell-Boeing V-22 *'Osprey'* rotorcraft has been shown to produce a brownout

Presented at 45th European Rotorcraft Forum, Warsaw, Poland, 17-20 September, 2019

This work is licensed under the Creative Commons Attribution International License (CC BY). Copyright © 2019 by author(s).

concentration of up to 3500 mg/m^3, several orders of magnitude greater than that which could be encountered naturally [3].

The operation of the rotorcraft itself exacerbates the concentration of the dust cloud due to the re-ingestion zone where the inflow through the rotor disk pulls the suspended dust back down towards the ground. This is significant because it typically occurs close to the helicopter's engine intakes, mounted high and forward on the fuselage. There is the added effect that rotorcraft operating close to the ground in a high power manoeuvre, which places a large mass flow requirement on the engine. This maximises the amount of particulates that are ingested compared to other engine power requirements.

Combining this with the high dust concentrations of a desert landing leads to the ingestion of large quantities of particulates. For example an engine with a mass flow rate of 16 kg/s would ingest up to 2kg of particulates during a 2 minute brownout landing manoeuvre. With the added context that a single platform tends to carry out these manoeuvres multiple times during a single mission, the cumulative quantity of dust ingested reaches a level which poses a serious concern to operators.

1.2. Turboshaft Engine Damage

Once particulates have been ingested, it can cause degradation and ultimately failure through multiple damage mechanisms in both the hot and cold sections of the engine.

The first components encountered by the dust are the low and high pressure compressors where particles can impact both vanes and rotors causing erosive removal of the substrate material. This erosion tends to be concentrated at the trailing edges of the blade tips where the normal velocities between particle and blade are at their greatest [4]. In addition, there is also an abrasive loss of material due to the rubbing of particles between the blade tips and the compressor casing. The result of this is an increase in the tip losses due to the additional flow leakage.

Operation of the compressor also has an impact on the particulates that pass into the latter sections of the engine. High rotational speeds cause milling and pulverisation, with individual particles being broken up into multiple fragments, skewing the size distribution of the dust to a smaller mean diameter compared to that ingested [5]. This milled dust enters the combustor where it is heated at temperatures typically between 1500K and 1800K and can either fully melt or partially soften during its residence. The softened particulates are then entrained in the combustor exit flow and enters the high pressure turbine where it can interact with and accumulate on the pressure surfaces of the first stage vanes [6].

Historically, particle ingestion during brownout has been mitigated against through the use of engine air particle separators (EAPS). When fitted to turboshaft engines, these systems have proved to significantly reduce the number of larger particles entering engines. However, regardless of the separator type, be this an inertial separator or a barrier filter, the efficiency of these devices reduces with decreasing particle size. In general, particles with equivalent spherical diameters less than 20 microns can be expected to evade inertial-type EAPS systems [7].

This paper looks to address how this 'pre-conditioning' of the particulates due to filtration and comminution processes in the sections of the engine preceding the turbine can affect the probability of safety critical damage occurring in the high pressure turbine. How this damage can be predicted using a statistical reduced-order model for nozzle guide vane deposition model and particulate sampling is also investigated. Finally, the suitability of different sampling locations and the effect that the sample collection location, either internal or external to the engine, has on the engine damage prediction is investigated.

1.3. NGV Particle Deposition Damage

The build-up of deposits causes distortion of the vane geometry as shown in Figure 2 and has two main effects that cause a reduction of both the aerodynamic and thermodynamic performance of the high pressure turbine. Firstly, there is a localised change in the surface roughness of the vane which causes early separation of the flow through the vane section, a reduction in the bulk flow velocity and a proportional reduction in the overall stage pressure drop [8]. Secondly, the physical thickness of the deposit causes a constriction in the nozzle passage of the vane, reducing the flow area and therefore flow rate through the engine core. Due to continuity this not only affects the local performance of the high pressure turbine, but has implications throughout the engine. The most significant consequence of this occurs in the compressor, which is required to operate at the same pressure ratio but a reduced flow rate, resulting in the working line shifting back towards the stability or surge line on the compressor map, reducing the surge margin of the engine [9]. It therefore follows that at some point, the thickness of deposit will reach a point that the combination of pressure ratio required and the restricted mass flow result in the working and stability lines converging, leading to a surge.

For the turboshaft engines typically fitted to

Presented at 45th European Rotorcraft Forum, Warsaw, Poland, 17-20 September, 2019
This work is licensed under the Creative Commons Attribution International License (CC BY). Copyright © 2019 by author(s).

rotorcraft the result of compressor surge would be loss of power during a critical stage of flight when it is needed most. This is a critical point as the turbine temperatures are also at their highest, increasing the probability of dust melting. Therefore, the event in which loss of power is most undesirable is also the point at which the damage mechanism inducing the loss of power is most probable. Indeed, it is thought that this susceptibility was the main cause in the fatal accident of a US Marines V-22 'Osprey' tilt-rotor aircraft which crashed due to sand deposition on the high pressure turbine nozzle guide vanes [10].

Figure 2: Dust deposition on a nozzle guide vane looking at the leading edge [11].

From the point of view of the turbine accretion damage mechanism discussed above, particles which evade the EAPS system are also the particle sizes which are likely to be suspended at heights that place them close to the engine intake and are therefore more likely to be ingested than larger particles. There is the added complication that the particle sizes in this range are likely to interact with internal components and are sufficiently small that they can melt or partially soften during their residence in the gas stream. This increases the likelihood that they will deposit on the vane during interaction, contributing to the NGV deposition damage mechanism that causes throat restriction and surface roughening.

2. BACKGROUND

2.1. Brownout Characterisation

The reduced visibility associated with brownout has led to a significant interest in studying the spatial distribution both of individual particles and the bulk concentration of the resulting clouds. A significant body of work was carried out during the US department of defence Sandblaster 2 testing campaign in which the brownout signatures of multiple rotorcraft were characterised [3]. This consisted of a range of particle samplers situated in multiple locations both radially outward from the rotor and vertically, giving the height profile of both the concentration and size distribution. These results are summarised for six rotorcraft and can be used to build up a picture of the dust cloud structure for these rotorcraft. The main finding of this study was the general conclusion that the severity of the brownout cloud concentration tends to scale proportionally with the disk loading of the rotor. This has since been shown to be dependent upon multiple parameters relating to both the rotor and the airframe, with the number of blades and wake strength having significant effects along with the blade tip design and fuselage shape [2].

Of the rotorcraft tested, five were of *'conventional'* configuration, the Bell UH1, Sikorsky HH-60, Boeing-Vertol CH-46, Sikorsky CH-53 and Sikorsky MH-53. The tilt-rotor architecture of the Bell-Boeing V-22 Osprey was also assessed. The determined bulk cloud concentrations at a height of 2 metres from the ground and 35 meters from the flight path line are presented in Table 1. Unfortunately, sampling was not carried out at a location more representative of the engine intake, where particles are ingested. As the vertical distribution of the cloud accounts for the particle size, with larger particles falling out of suspension more rapidly, capturing this in the concentration and size distribution was prioritised over using particle size data from a sampling location closer to the rotor disk but on the ground, where this settling effect would not be captured.

Table 1: Brownout concentrations at a height of 2m and 35 m from the rotor disk, extracted from the Sandblaster 2 study data along with the corresponding disk loading of the rotorcraft.

Rotorcraft	**Brownout Concentration, C_p, $[mg/m^3]$**	**Disk Loading, D, $[N/m^2]$**
UH-1	334	239
HH-60	2089	287
CH-46	476	383
CH-53	3326	479
V-22	3468	958
MH-53	3194	479

The V-22 is significant from a brownout perspective as its disk loading of 960 N/m^2 is

Presented at 45th European Rotorcraft Forum, Warsaw, Poland, 17-20 September, 2019
This work is licensed under the Creative Commons Attribution International License (CC BY). Copyright © 2019 by author(s).

almost double that of the most highly loaded conventional rotor tested (CH-53: 479 N/m^2) and therefore is believed to suffer more significantly from brownout related engine degradation. However, when studying the results of the Sandblaster 2 tests presented in Table 1 we see that the MH-53 has a comparable brownout concentration to the V-22, suggesting that conventional rotorcraft with large number of blades (six for MH-53) may also be prone to flame out from major dust ingestion events.

2.2. Mass Deposited on an NGV

A first order approximation of the damage experienced by a nozzle guide vane is often the determination of the total mass of deposited material that builds up. An empirical model has been proposed by Clarkson and Simpson which allows this to be described so long as appropriate empirical parameters are understood [9]. The rate at which mass accumulates on a vane can be described analytically as:

$$\frac{dm_p}{dt} = \frac{C_p\,\zeta_{NGV}}{\rho_f} \tag{1}$$

Where C_p is the concentration of the particulates cloud that is encountered and ρ_f is the air density. The key parameter in this equation, ζ_{NGV} is the *'accumulation factor'* of the particulates ingested. This is the mass fraction of dust ingested by the engine which ultimately deposits on the surface of the vane. It depends upon multiple factors relating to the size, shape and composition of the bulk dust. The study of accumulation factors for mineral dusts is scarce, however, work has been undertaken to identify accumulation factors which result in engine surge for volcanic ashes. Analysis of historical aircraft encounters has shown that an accumulation factor as low as 6% is sufficient to surge an engine [12]. With the knowledge that the accumulation factors of mineral dusts are generally smaller than those for ash, this can be taken as an overly conservative estimation of the sand/dust accumulation factor required to cause surge [13].

Then for a finite exposure time to the concentration of particulates, C_p, the mass deposited on a vane can be described as a function of the particle 'dose'. This is defined as the product of the concentration and the exposure time, Δt.

$$\delta_p = C_p \Delta t \tag{2}$$

The dose allows damage occurring at different combinations of duration and concentration to be compared. Currently, this damage classification is carried out qualitatively using the metrics defined by Clarkson and Simpson [9]. This metric defines broad boundaries describing damage levels which result in significant safety implications such as complete loss of engine power, exigent damage which would require an engine to be repaired post-flight, and long term economic damage.

This work aims to begin to quantify the damage which manifests as throat restriction and surface roughening for different 'doses' of particulates, constituting a shift from this qualitative metric to a quantitative one.

2.3. DEvAC Chart

The simple analytical model of Clarkson and Simpson [9] has been used to carry out a systematic assessment of known aircraft-particulate encounters based upon the dose encountered and the qualitative extent of engine damage experienced. This has been shown graphically in the form of the DEvAC chart (Fig. 3), which plots the concentration against duration of a particular encounter as a series of ellipses. The size of the ellipse denotes the uncertainty in either the concentration or duration of the encounter.

Limits are also included which identify likely regions of safe and unsafe operation in volcanic ash. How these boundaries relate to operations in sand and dusts is unknown, although it is expected that these boundaries would be pushed to higher concentrations and durations due to the generally less damaging nature of crystalline mineral dusts/sands [14] and therefore can expect lower accumulation factors for these dusts. The non-linear shape of these boundaries accounts for the fact that whilst material can accumulate on the turbine vanes, it can also be aerodynamically shed.

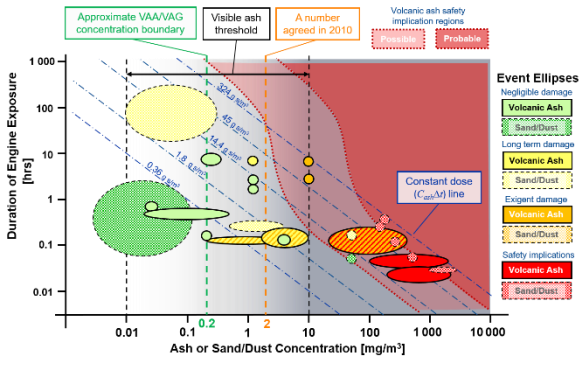

Figure 3: The Duration of Exposure versus Ash Conentration (DEvAC) chart.

Presented at 45th European Rotorcraft Forum, Warsaw, Poland, 17-20 September, 2019

This work is licensed under the Creative Commons Attribution International License (CC BY). Copyright © 2019 by author(s).

Clarkson and Simpson noted that at high concentrations, this shedding effect is overcome by particle sticking and therefore a particle mass that can cause safety concerns is reached more rapidly. By contrast, at lower concentrations, the shedding and accumulation mechanisms reach a point where they are relatively constant and there is a steady mass built up on the vane. Reducing the concentration and increasing the exposure further, the shedding mechanism is the dominant factor and engine failure in this region is instead driven by degradation of the compressor.

The rationale behind the DEvAC chart is to allow a comparison of different aircraft-particulate encounter events. The use of the dose in doing this allows events occurring at different combinations of concentration and duration to also be compared. The comparison that is carried out is based upon a qualitative assessment of the damage experienced during a particular encounter. This assessment is carried out from visual evidence of engine components and the observed changes in engine performance trends. The damage categories range from *'negligible damage'* in which there is no evidence that the aircraft has encountered particulates, through *'long term'* and *'exigent'* damage, which correspond to visible damage that does not affect performance to damage that results in a noticeable performance deterioration but does not impact operating safety limits. The final damage category is *'Safety Implications'* which corresponds to scenarios in which there is a total loss of engine power.

2.4. Particle Size Distributions

As has already been discussed, the brownout clouds produced by rotorcraft can exhibit a range of particle sizes due to the inertial sorting mechanisms that occur within the cloud and which are dependent upon the rotor design. The result of this is that the particle size distribution exhibited within the cloud can vary, depending on the sampling location and sampling height.

In general, most particle size distributions can be represented using a statistical function describing the number of particles in a sampled mass of particles that fall within a particular range of diameters or 'bin'. An example of this is the standard log-normal distribution for which the mass fraction, m_f of particles with diameter, d_p takes the form:

$$m_f = \frac{1}{d_p \sigma \sqrt{2\pi}} \, exp\left(-\frac{\left(ln(d_p) - \mu\right)^2}{2\sigma^2} \right) \tag{3}$$

Where σ and μ are the standard deviation and mean of the distribution respectively.

As has already been discussed, the particle size distribution that enters the first stage of the turbine is unlikely to be that which enters the engine intake or that which is sampled from the bulk dust cloud. This is due to the presence of sorting mechanisms, both intended and unintentional due to the operation of the engine.

The extent of the sorting process in the EAPS system is well understood and the upper diameter limits this places on the particle size distribution at turbine entry are well understood [7]. Beyond this, the effect that milling and fragmentation of individual particles has on the size distribution is still an open area of research.

3. METHODOLOGY

3.1. Reduced Order Engine Damage Model

A reduced order particle-vane accumulation model has been developed in a statistical form to relate non-dimensional properties of the particle to its probability of depositing on a nozzle guide vane. The overall likelihood of deposition is defined as the capture probability for the particle and is split into two separate probabilities which combine to give the capture probability. When evaluated for a range of particles with varying size this gives the overall accumulation factor, ζ_{NGV} which can be used in Equation 1 to determine the total mass of deposit that accumulates on a vane.

The interaction probability is defined as the likelihood of a particle following a trajectory through the nozzle guide vane stage such that it comes into contact with the vane. It is a function of the particle inertia and depends primarily upon instantaneous inertial drag force acting on the particle. The interaction probability has been shown by Bojdo et al. [11] to vary depending upon multiple properties relating to both the gas and particle which result in drag non-linearity depending upon the trajectory followed. To address this, the authors developed a new form of the classical Stokes Number, including an existing correction factor which accounts for drag non-linearity over a range of turbine operating conditions. This result was a new 'generalised' Stokes number which takes the form:

$$Stk_{in} = \frac{\rho_p d_p}{18} \left(Re_p \psi\right)(Nh) \frac{U_{in}}{\dot{m}_{core}} \tag{4}$$

Where ρ_p, d_p, Re_p are the density, diameter and relative Reynolds number of the particle. The variables N & h are stage design parameters, the number and height of the NGV's respectively.

Presented at 45th European Rotorcraft Forum, Warsaw, Poland, 17-20 September, 2019

This work is licensed under the Creative Commons Attribution International License (CC BY). Copyright © 2019 by author(s).

Finally, operating parameters, the core mass flow rate $\dot{m}_{core}$ and flow inlet velocity, U_{in} are included

The work of Bojdo et al. [11] showed how two-dimensional CFD simulations can be used to produce a reduced order function describing the retention probability of particles with different generalised Stokes numbers. The method presented results in a single function for all particles is dependent only on the particular vane geometry and the particle shape. The resulting function takes the hyperbolic tangent form given by Equation 5:

$$\chi = \left(\boldsymbol{a}\tanh\left(\boldsymbol{b}\,Stk_{gen}{}^{\boldsymbol{c}}\right)\right) + \boldsymbol{d} \tag{5}$$

Where the coefficients a, b, c and d are determined through a regression analysis of the CFD results.

The second facet of the model is the probability of a particle being retained if it comes into contact with the vane; termed the *'retention probability'*. This depends on the physical state of the particle and broadly a measure of how *'soft'* it is upon interaction, with softer particles being more likely to be retained. This is dependent upon the composition of the bulk particulates, with high silica content mineral dusts generally resulting in a reduced probability of retention compared to amorphous ash type materials. In order to implement this within the CFD modelling used to develop reduced order functions, a 'particle fate model' is required which describes the conditions under which a particle is retained.

The retention model used in the CFD simulations is the elastic-plastic impact and deformation model developed by Bons et al. [13], based around the normal kinetic energy of the particle. This is the most complex particle retention model derived to date as it accounts for combined elastic-plastic impact behaviour. By comparison, previous modelling considered only elastic collisions. This is an important concern for particle fate models, as particles which impact with large normal kinetic energies are likely to undergo plastic deformation. This is due to the fact that they can only store a finite amount of energy elastically, before any other energy loss is dissipated during plastic deformation to permanently change the shape of the particle. Crucially, this energy cannot be recovered and used to rebound; particles which deform plastically are more likely to be retained by the vane. This effectively places an upper limit on the available energy that can be used by the particle to rebound after the initial impact which is given mathematically by:

$$E_{crit} = \frac{{\sigma_y}^2 {d_p}^2}{8G_p} \tag{6}$$

Where σ_y, d_p and G_p are the yield strength, diameter and elastic modulus of the particle.

The particle retention model accounts for two additional physical mechanisms which influence the energy of the particle available post impact. The first of these is the adhesion between the particle and vane surface, with the bond strength, W_a taking the same form stated by Bons et al [13]. It is assumed that the particle bonds to the substrate instantaneously on impact and to break this bond the particle must possess sufficient kinetic energy which outweighs the bond strength. The second mechanism is the removal of particles due to shear flow in the boundary layer. This takes the form given by Bons et al. [13] and determines the moment and therefore energy required to remove a particle, M_{drag}. Mathematically it is incorporated as an additional energy available to the particle during the rebound phase and is simply added to the energy available once adhesion energy is accounted for. Due to the upper limit placed on the elastic energy storage for either elastically or plastically impacting particles, the rebound energy of the particle is determined using the following:

For elastic impacts:

$$E_2 = E_1 - W_a + M_{drag} \tag{7}$$

For plastic impacts.

$$E_2 = E_{crit} - W_a + M_{drag} \tag{8}$$

Finally, the initial kinetic energy of the particle is compared to that determined using either Equation 7 or Equation 8 to give the coefficient of restitution of each individual particle:

$$CoR_n = \sqrt{\frac{E_2}{E_1}} \tag{9}$$

Particles with a coefficient of restitution equal to zero are therefore retained by the vane and contribute towards the accumulation factor of the bulk dust. Those with non-zero coefficients of restitution rebound on impact with their rebound velocity calculated from their normal kinetic energy after impact

Implementation of this model in the CFD simulations used in the interaction probability

Presented at 45th European Rotorcraft Forum, Warsaw, Poland, 17-20 September, 2019

This work is licensed under the Creative Commons Attribution International License (CC BY). Copyright © 2019 by author(s).

determination allows the retention probability of a single particle diameter with the vane to be determined. The resulting retention probability for a given particle diameter can then be expressed in terms of the corresponding thermal Stokes number. This is a non-dimensional thermal response time which accounts for the physical state of the particle through the inclusion of the bulk softening temperature of the material, T_{soft}.

$$Stk_{th} = \frac{c_{p,p}\rho_p{}^2 k_p d_p{}^2 \mu_f}{12 k_f{}^2 \rho_f{}^2 L_{th}{}^2} \frac{T_{p,soft}}{T_{p,in}} \quad (10)$$

Using this Thermal Stokes number, the probability of retention determined from each of the CFD simulations can be fit using regression analysis and the same hyperbolic tangent function as the interaction probability (Eq.5). As with the interaction probability, there are limits to the applicability of this reduced order function. The retention probability is determined for a given gas temperature, particulate type and NGV geometry.

$$\xi = (\boldsymbol{a} \tanh(\boldsymbol{b}\, Stk_{th}{}^{\boldsymbol{c}})) + \boldsymbol{d} \quad (11)$$

Finally, we can combine Equation 5 with Equation 6 for a particular particle to give its accumulation factor as:

$$\zeta_{NGV} = \chi . \xi \quad (12)$$

This represents the accumulation factor of a single particle, but the same method can be applied to a particle size distribution containing a range of diameters in varying proportions. Bojdo et al. [11] showed how the interaction probability can be used to determine the bulk *'interaction factor'* of a size distribution by multiplying the mass proportion of each diameter in the dust with its corresponding interaction probability. Carrying out the same process for the retention probability yields the *'retention factor'* and combining these gives the overall accumulation factor, $\zeta_{NGV}$of the dust distribution for a given vane, particle type and flow condition.

3.2. Particle Properties

Whilst the Sandblaster 2 study carried out an extensive analysis of the brownout cloud concentration and size distribution for six different rotorcraft, no analysis was carried out on the composition of the dust at the Yuma proving ground. As identified above, it is this composition which is the main factor in determining the probability of retention of a particle and therefore multiple inputs relating to the elastic and thermo-physical properties of the particle are required by the particle fate model. The Sandblaster testing campaign was carried out at the La Posa drop zone of the Yuma Proving Ground in Arizona, United States. Unfortunately, the composition and bulk properties of this particulate are not reported in the wider literature as this fell outside the objectives of their study. For the analysis carried out in the present work, we instead assume that the properties of the Yuma dust are analogous to those of the standard Arizona Road Dust which are widely reported in the literature and are summarised in Table 2:

Table 2: Bulk elastic and thermal properties of Arizona Road Dust.

Property	Value	Ref.
Bulk Density, $\rho_p, [kg/m^3]$	2650.00	[13]
Heat Capacity, $c_{p,p}, [J/kgK]$	679.00	
Thermal Conductivity, $k_p, [W/mK]$	5.40	
Yield Strength, $\sigma_y, [Pa]$	1.10E+11	[15]
Elastic Modulus, $G_p, [Pa]$	1.29E+11	[13]
Poisson Ratio, $\nu_p, [-]$	0.16	
Free Energy, $\gamma_p, [-]$	0.80	

The final particle property that must be specified in the particle retention model is the rate at which the particle yield strength reduces with increasing gas temperature. It is suggested by Bons et al. that this takes the form of Equation 13, a linear reduction with temperature [13]:

$$\sigma_y = G_p - B(T_p - T_f) \quad (13)$$

Where G_p is the *'baseline'* yield strength of the particle given in Table 2 and B is the gradient coefficient for the linear reduction, determined using experimental data fitting. Unfortunately, the data required to carry out this fitting does not exist for Arizona Road Dust, so the value of 0.225 quoted by Bons et al. for ash particulates is used in lieu [13]. Finally, T_f is the temperature of the fluid surrounding the particle. This function is implemented in the particle fate model to instantaneously update the particle yield strength at each point along its trajectory. With reference to Equation 6, we can see that as the yield strength reduces with increasing temperature, the critical elastic energy storage also reduces. The result of this is that the number of particles which deform plastically and therefore deposit increase. It is

Presented at 45th European Rotorcraft Forum, Warsaw, Poland, 17-20 September, 2019
This work is licensed under the Creative Commons Attribution International License (CC BY). Copyright © 2019 by author(s).

through this process that the trend of increasing deposition with temperature is incorporated into the particle fate model.

Using the properties in Table 2, the inertial and thermal Stokes numbers can be determined for a range of particle diameters in a size distribution. For the interaction probability, the coefficients determined by Bojdo et al. [11] for the interaction of spherical particles with the General Electric Energy Efficient Engine (GE-E^3) NGV are used in the absence of an NGV geometry for any of the engines used in the Sandblaster study.

Table 3: Coeffieicnts used for the reduced order model interaction probability function.

	Coefficients			
	a	**b**	**c**	**d**
$\eta_{interact}$	-0.961	-2.700	1.600	0.039

To evaluate the retention probability of the particle, a user defined function of the particle fate model described in Section 3.1 was implemented into CFD simulations of the same GE-E^3 NGV. This used the properties of Arizona Road Dust given in Table 2, allowing a regression analysis to determine the probability of retention as a function of thermal Stokes number for four different continuous phase temperatures. The coefficients for Equation 11 and their corresponding thermal Stokes number range are given in Table 4.

Table 4: Coefficients used for the reduced order model retention probability function with varying gas temperature.

		Coefficients			
T [K]	Stk_{th} Range	**a**	**b**	**c**	**d**
1400	0 - 15	-0.91	-0.07	-1.32	0.09
	15 - ∞	-0.15	-5.65	-0.76	0.00
1500	0 - 6	-0.86	-0.04	-1.80	0.14
	6 - 15	-0.21	-3E-7	5.40	0.14
	15 - ∞	-0.27	-3391	-2.02	0.00
1550	0 - 8	-0.82	-0.04	-1.95	0.12
	8 - 55	-0.49	-1E-6	4.68	0.17
	55 - ∞	-0.70	-700	-1.50	0.00
1600	0 - 5	-0.84	-0.08	-1.3	0.16
	5 - 21	-0.86	-8E-5	3.43	0.15
	21 - ∞	-1.00	-900	-1.50	0.00

4. RESULTS

4.1. Sandblaster 2 Analysis

The results from testing to determine the brownout signatures of rotorcraft used in conjunction with the reduced order NGV damage model described in Sections 3.1 and 3.2 can provide an insight into the extent of deterioration that can be expected in an engine whilst operating in brownout conditions. The Sandblaster 2 study previously discussed is one of these sources. To be able to begin estimating the extent of damage that could be expected in the engines of these rotorcraft, five main properties of the dust cloud are required:

- Cloud Concentration
- Particle Size Distribution
- Exposure Duration
- Particle Composition
- Particle Bulk Properties

The published particle size distributions of Cowherd Jr. [3] sampled at different points in the dust cloud can be used to provide an approximation of the first two of these parameters. The third can be inferred from the flight speeds and the documented length of the sampling set-up. Finally, the more complex of these is the composition of the particulate and its resulting bulk properties. As has already been discussed, the bulk properties and composition of the Yuma dust are not available in the open literature and therefore for the work presented here it is assumed analogous to the standard Arizona Road Dust.

4.1.1. Dose Approximation

Using the presented data from the Sandblaster 2 study, it is possible to derive a corresponding dose received by each rotorcraft in the study. Three *'runs'* were carried out with each platform. We present the cumulative dose accumulated over all flights. Using the length of the sampling set-up and the provided flight speeds for each test, the duration in brownout can be derived for each test run. These are then simply added to give the cumulative dose received by the engine presented in Table 5. We also include the already discussed V-22 accident in Oahu as a reference for an event in which the damage sustained was sufficient to cause engine failure. In this case we use available evidence from Sweetman [10] which suggests that the crashed V-22 was exposed to an estimated core particle dose of 496 gs/m^3. This is based upon video evidence of the event and the assumed brownout concentration from the Sandblaster 2 testing.

Presented at 45th European Rotorcraft Forum, Warsaw, Poland, 17-20 September, 2019
This work is licensed under the Creative Commons Attribution International License (CC BY). Copyright © 2019 by author(s).

Table 5: Dose approximation for the rotorcraft in the Sandblaster 2 study.

	Brownout Concentration C_p, $[mg/m^3]$	**Cumulative Duration** Δt, $[s]$	**Total Dose** δ_p, $[gs/m^3]$
UH-1	334	117	39.1
HH-60	2089	57	119.1
CH-46	476	51	24.3
CH-53	3326	57	189.6
V-22	3468	117	405.8
MH-53	3194	147	470.0
V-22 (Oahu)	3468	143	495.9

Using the dose presented in Table 5 for each rotorcraft and their corresponding concentration and duration, we can then include these events on the DEvAC chart to draw comparison with other sand/dust encounters. The lower concentration limit of the Sandblaster ellipse is set by the UH-1 and the upper limit set by the MH-53 concentration of 3326 mg/m^3. The first thing we observe is that the encounters are all relatively short duration and high concentration exposures as would be expected. This places them in the bottom right corner of the chart where we have already identified that the primary mechanism for engine failure is surge due to turbine deposition and throat area reduction.

In terms of the safety implications of this, the combination of concentration and duration for the cumulative Sandblaster tests on each airframe places these events in the *'possible safety implications'* region although it should be noted that this is a limit established for volcanic ash, a particulate understood to accumulate more readily than mineral dusts. This limit is also based upon large civil turbofan engines which have different engine architectures to military turboshaft engines. The most notable of these is the presence of the EAPS system commonly fitted to rotorcraft to protect from FOD ingestion. It is expected that the effect of this and the ingestion of mineral dust rather than volcanic ash would be to shift the boundaries to higher concentrations and durations for comparable levels of damage.

Unfortunately, the damage suffered by the engines in the Sandblaster 2 study is undocumented and so the extent of damage cannot be evaluated either qualitatively or quantitatively. As a measure of comparison with an encounter for which the safety implications are known, we include the V-22 encounter in Hawaii in the DEvAC chart. It is known that this encounter resulted in engine surge and loss of power. Therefore it can be classed as an event with *'safety implications'*. This is evidenced by the fact that this incident falls inside the *'probable'* safety implication region. This is an interesting result as it suggests that the boundary for this safety implication region may be appropriate. However, we see that the cumulative effect of the three tests carried out using the V-22 in the Sandblaster 2 test also approaches this boundary, suggesting that this testing campaign could have resulted in similar consequences, if the dust were the same.

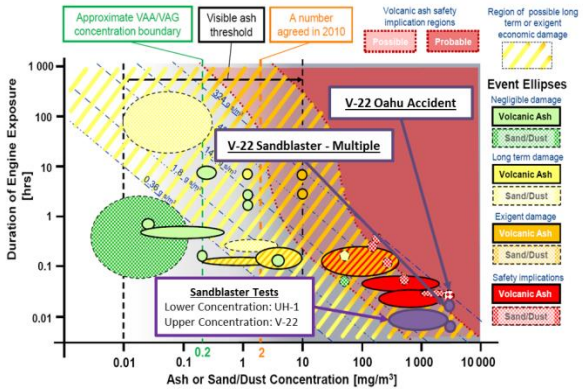

Figure 4: Revised DEvAC chart including results from the Sandblaster 2 testing campaign and the 2015 V-22 accident in Hawaii.

4.1.2. Particle Size Distributions

The sampling data collected during the Sandblaster 2 campaign and used to determine the concentrations presented in Table 1 also allowed the particle size distribution of the dust cloud to be determined for each rotorcraft. This was analysed by manually micro-sieving the collected dust down to a range of diameters and comparing the mass collected in each sieve to the total mass collected. The sieve sizes used represent the particle size *'bins'* that are reported in the distribution data. A total of 9 sieve screen sizes were used with the smallest corresponding to 1 micron diameters.

The data reported by Cowherd Jr. [3] for particle mass fractions by size in the 2m tower sampler can be fitted with a Log-Normal distribution of the form given by Equation 3. A regression analysis has been carried out on the particle size data for each of the rotorcraft in the study to determine the

Presented at 45th European Rotorcraft Forum, Warsaw, Poland, 17-20 September, 2019
This work is licensed under the Creative Commons Attribution International License (CC BY). Copyright © 2019 by author(s).

corresponding mean and standard deviation of the fitted distribution. The parameters of these distributions are presented in Table 6.

Table 6: Summary of Log-Normal distribution parameters for the sampled particle size distributions in the Sandblaster 2 study.

Rotorcraft	Mean μ	Standard Deviation σ	Coefficient of Determination R^2
UH-1	47.22	2.12	0.89
HH-60	80.92	2.25	0.78
CH-46	60.57	2.29	0.82
CH-53	79.18	2.01	0.85
V-22	56.30	2.32	0.91
MH-53	63.46	2.09	0.91

Also included in Table 6 is the goodness of fit measure, giving an indication of how suitable the Log-Normal fit is for the sampled data. This is evaluated using the Coefficient of Determination, R^2 which gives a measure of the predictability of the output variable from the input variable; in this case, the predictability of the mass fraction from the particle diameter. The results in Table 6 show that the log-normal distribution provides a relatively good fit for all of the brownout clouds sampled.

An example of the fitted log-normal distribution for the V-22 'Osprey' is shown in Figure 5 for which the mean diameter in the distribution is 56.3 microns with a standard deviation of 2.32. We maintain this distribution and variations of it for the future analysis using the reduced order model.

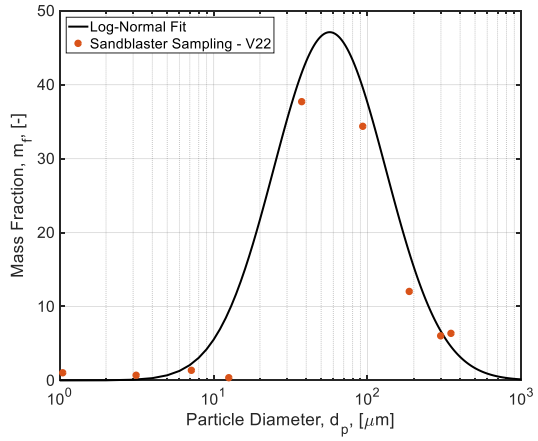

Figure 5: Fitted Log-Normal distribution for the measured particle size distribution of the V-22.

By comparing the results in Table 6 with the brownout cloud concentrations in Table 1 we see that for the conventional rotorcraft, the increasing concentration and rotor disk loading results in an increase in the mean particle diameter of the dust cloud produced. The lightly loaded rotor of the UH-1 exhibits the smallest mean particle size. This can be attributed to its relatively low wake strength which reduces the strength of the vortices which bundle causing the long-term suspension of larger particles. By contrast, the CH-53 produces the distribution with the largest mean diameter, something understandable given that it has the highest disk loading of the conventional configutration rotorcraft tested and therefore the strongest suspension mechanism [2].

The case of the V-22 Osprey tilt-rotor in these results does not follow the trend exhibited by the conventional configuration rotorcraft. It shows a relatively modest mean diameter of 56.3 microns. However, it also posseses the largest standard deviation of all the platforms tested and therefore the largest range of diameters in its size distribution. The result of this is that the proportions of the particles which can be expected to evade an EAPS system and reach the engine core will exist in larger proportions in the V-22 brownout cloud than for the other rotorcraft. This could go some way to explaining the susceptibilty of the V-22 to engine degradation during brownout conditions.

4.1.3. Reduced Order Model Application

Taking the size distribution fitted in Figure 5 for the V-22 we can use the reduced order particle deposition model described in Section 3.1 to determine the proportion of particles in the distribution that stick to the vane and therefore the accumulation factor.

For each diameter in the size distribution, we determine the corresponding interaction and retention probabilities using Equations 5 & 11 respectively. The coefficients used in these equations are those from Table 3 for the interaction probability and the 1600K coefficients for the Arizona Road Dust in Table 4. It should be noted that these coefficients are for GE-E^3 NGV and not that of the exact V-22 engine NGV geometry. These functions provide the curves which bound the shaded regions labelled *'Interacted'* and *'Potentially Retained'* in Figure 6. The latter of these is only *'potentially'* retained as some of these particles may ultimately never interact with the vane. Combining these two probabilities and multiplying by the mass fraction gives the capture probability for each diameter in the distribution, represented by the dark grey

Presented at 45th European Rotorcraft Forum, Warsaw, Poland, 17-20 September, 2019
This work is licensed under the Creative Commons Attribution International License (CC BY). Copyright © 2019 by author(s).

shaded *'captured'* region of the plot. By comparing the area of this region to the area under the whole particle size distribution, we obtain an accumulation factor for the diameter under consideration.

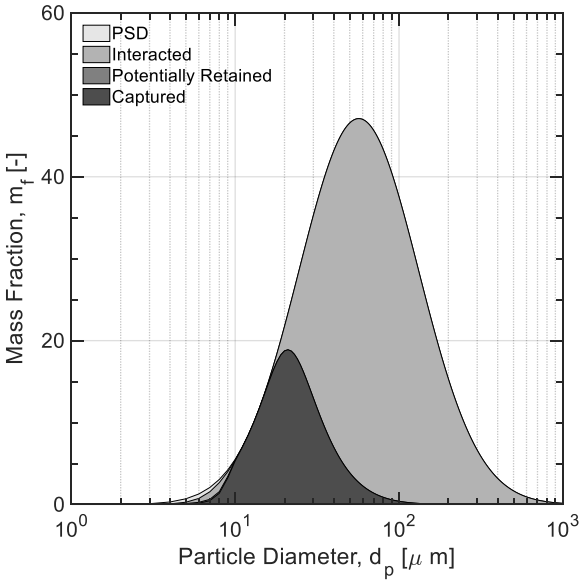

Figure 6: Graphical representation of the accumulation factor for the V-22 particle size distribution.

Due to the fact that the smallest sampled diameter is around 1 micron, we see that the vast majority of this sample is likely to interact with the vane, and all of that which has the potential to be retained is indeed captured. The result is an accumulation factor of 6.72%. This is within the 5-15% range of accumulation factors reported by Clarkson et al. as potentially being sufficient to cause engine surge in large civil turbofan engines [12]. This may seem low when comparing the area under the two curves, however it should be noted that this is a mass based accumulation factor and as the majority of retained particles are the smallest in the PSD this therefore represents a much smaller proportion of the total mass in the PSD.

It is also unknown how this accumulation factor would compare to that required to cause a turboshaft engine to surge. What is understood is that the accumulation factor presented here is for an un-modified dust distribution that does not take into account the various sorting processes which occur in earlier stages of the engine and result in a reduction of the mean diameter in the size distribution. With this change in PSD through the engine, we would therefore expect the accumulation factor to change too. This is due to the fact that as the size of particle generally gets smaller, their interaction probability reduces and hence so does their probability of being captured.

Whilst the process demonstrated here has been applied to a dust sample collected relatively far away from the rotorcraft and the centre of the dust cloud, where the engine intake is located, the same approach could be just as simply applied to any other particle size distribution collected either inside the engine at different stages during routine maintenance, similar to that carried out by Wood et al. [16], or at its intake.

Of these two possibilities, sampling from the engine intake is the most practical and the easiest to use to carry out assessments of the engine damage. We therefore seek to use this reduced order model to understand what processes would need to occur to the sampled particle size distribution in the preceding sections of the engine such that the damage experienced is sufficient to surge the engine.

4.2. Accumulation Factor to Surge

We know that the particle separator systems fitted to most rotorcraft result in an upper limit being placed on the maximum particle size that enters the core of the engine. This boundary varies depending upon the type of particle separator that is employed.

To investigate this effect, we exercise the reduced order model with a range of particle size distributions based upon the sampled V-22 PSD from the Sandblaster 2 work. To do this, we assume that the fragmentation through the compressor produces a size distribution with the same standard deviation as the ingested dust, but a reduced mean diameter. This results in the overall *'spread'* of the distribution increasing, and therefore the mass fraction of each diameter reducing with decreasing mean particle size. This is because the distribution now covers a wider range of particle sizes, however, the area under the distribution does not change as the total mass of particles remains constant. The effect of particle fragmentation is modelled by defining a series of *'processed'* size distributions. These are based upon the 'raw' PSD for the V-22 shown in Figure 5. A range of 10,000 mean particle diameters are defined between 0.1 and 100 microns. The result of this is 10,000 log-normal size distributions each with a different mean diameter between 0.1 and 100 microns, but with all distributions having the same standard deviation. These distributions are evaluated over particle diameters ranging from 0.01 to 1000 microns using Equation 3. This gives the corresponding mass fraction. A sub-set of these distributions for mean diameters of 2.5, 7.5 and 20 microns are shown along with the original V-22 PSD in Figure 7.

Presented at 45th European Rotorcraft Forum, Warsaw, Poland, 17-20 September, 2019
This work is licensed under the Creative Commons Attribution International License (CC BY). Copyright © 2019 by author(s).

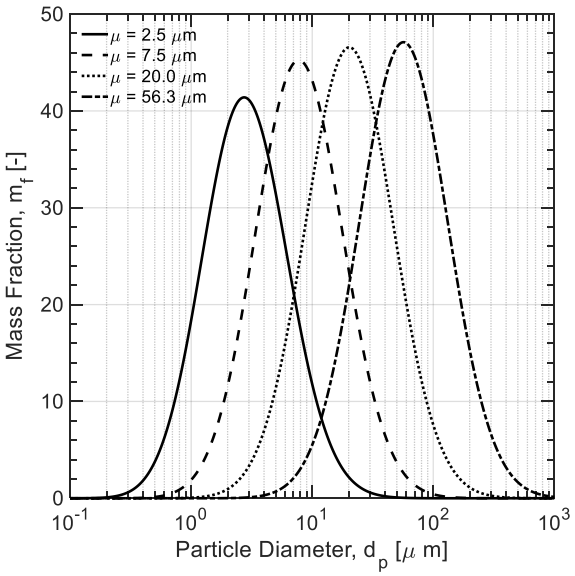

Figure 7: Subset of derived distributions for the V-22 brownout, idealising the effect of the compressor fragmentation mechanisms on the mean particle size in the distribution.

For each of the 10,000 distributions, we then use the coefficients shown in Table 3 and Table 4 to apply the reduced order model and determine the interaction and retention probabilities for all particles in each of the size distributions. We then use this to calculate the accumulation factor for each of the distributions using the same approach as in Section 4.1.3. Carrying out this process for each of the four temperatures gives the curves which comprise Figure 8. This shows how the mean diameter of the log-normal distribution affects the accumulation factor of the dust. How the accumulation factor varies for each distribution presented in Figure 7 at different turbine entry temperatures is summarised in Table 7. Also included are the range of mean diameters that result in surge ($\zeta_{NGV} > 0.06$) for each temperature.

Table 7: Calculated accumulation factors for the distributions presented in Figure 7 with increasing turbine entry temperature and the mean diameters that can be expected to result in surge.

Mean Diameter $\mu, [\mu m]$	**Temperature** $T, [K]$			
	1400	1500	1550	1600
	Accumulation Factor $\zeta_{NGV}, [-]$			
2.5	3.9	9.9	20.8	33.2
7.5	3.9	12.3	34.4	55.7
20	2.3	7.0	25.6	42.1
Mean Diameter for Surge $\mu, [\mu m]$	-	1.4 - 24	0.9 - 295	0.7-5000

In Figure 8 we plot the calculated accumulation factors for all 10,000 distributions at each temperature and include the previously noted limit that accumulation factors of 5-15% can be sufficient to surge a large turbofan engine which ingests volcanic ash. These limits are indicated by the two horizontal lines on the graph. We can also place limits on the mean diameters we expect to see for representative particle size distributions in the high pressure turbine. Clarkson et al. [12] noted that in general, particles larger than 6-7 microns are unlikely to be present in the latter stages of the engine due to fragmentation in the compressor. However, these limits are for large turbofan engines and the type of particulate is not quoted. For turboshaft engines, a well understood limit is the EAPS maximum diameter which can range from 20-40 microns depending on the system architecture. This is also included for reference. We can see in Figure 8 that the accumulation factor peaks at a given mean diameter. As expected, the peak accumulation factor increases with temperature and occurs at a slightly larger mean diameter as the temperature increases. This is due to the reduced yield strength of the particles with temperature (Eq. 13) which increases their probability of being retained. The increase in accumulation factor from 0.1-7 microns is followed by a reduction in the accumulation factor after the peak. This decrease is driven by the fact that that larger particles are more likely to exceed the critical energy storage and deform elastically (Eq. 6). They are therefore less likely to be retained. As such, when we increase the mean diameter of the log-normal distribution, the mass fractions of relatively *'larger'* particles increase and therefore the accumulation factor for the distribution as a whole reduces.

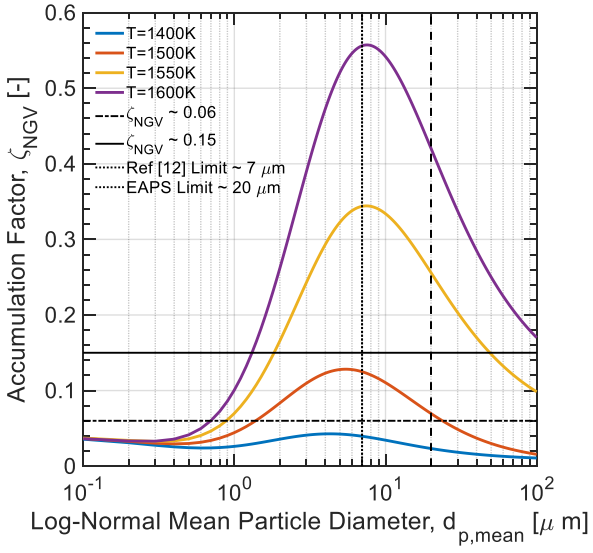

Figure 8: Accumulation factor versus mean particle diameter for a range of turbine entry temperatures.

Presented at 45th European Rotorcraft Forum, Warsaw, Poland, 17-20 September, 2019
This work is licensed under the Creative Commons Attribution International License (CC BY). Copyright © 2019 by author(s).

In the absence of surge accumulation factor for mineral dusts and turboshaft engine architectures, we can take the limits given for large turbofans exposed to volcanic ash and apply them in the knowledge they are likely to be conservative estimates of the expected damage. This allows Figure 8 to be analysed in terms of the engine damage that can be expected and the risk associated with certain operating conditions to be analysed. In Figure 9 we grade areas of the chart from green – damage unlikely through to orange for potential damage and finally to red where engine damage is highly likely. The grey shaded area to the right of the figure represents the EAPS particle diameter limit, above which it would be unlikely to obtain a log-normal size distribution with these mean diameters.

It is envisaged that with appropriate limits determined for the upper particle size limit and representative accumulation factors required to cause surge for the ingestion of mineral dusts that these charts can be used to inform a graduated risk approach to operations in dusty environments. It is clear from this that any sample taken either form the ground or in an engine can be analysed using this method and used to determine the expected damage and therefore any potential safety implication of operating rotorcraft in a particular region.

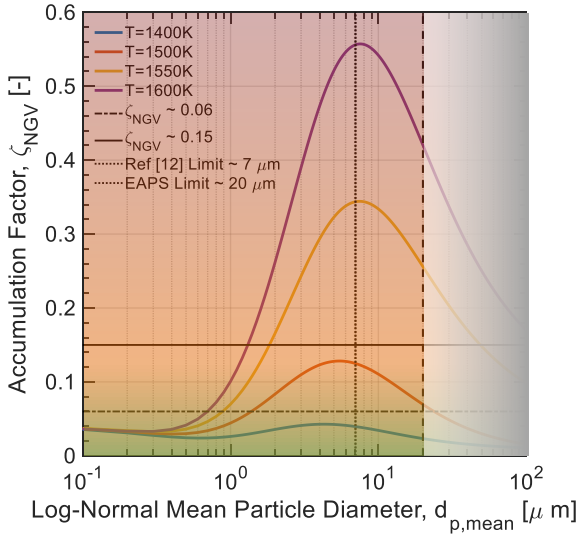

Figure 9: Re-presented form of Figure 8 showing the regions of high and low likelihood of NGV damage.

5. CONCLUSIONS

A methodology has been presented which allows the damage expected during brownout conditions to be determined from the in-service sampling of dust clouds. This allows an accumulation factor to be estimated based on the mean particle diameter and composition of the sample. It has also been shown how this methodology can be used to provide operational awareness to planners and crews via a graduated risk approach to ensure that the accumulation factor endured does not exceed a pre-defined limit above which engine surge could be possible. To be able to carry out this assessment with confidence, indicative accumulation factors which result in surge are not well understood for turboshaft engines subjected to mineral dust ingestion. It is expect that these limits will be greater than those discussed in this contribution for volcanic ash and large turbofans.

Currently, the main limitation of this method is that the particle retention model used in the reduced order model requires the specification of temperature dependent elastic properties of the bulk particulates. This is the method through which the increase in accumulation factor with turbine entry temperature is captured. A method is therefore required through which these functions can be determined and incorporated into the model. Additional limitations still exist in the model, most notably being able to represent how the PSD sampled either in the bulk dust cloud or at engine inlet relates to that on entry to the high pressure turbine. Although this could be avoided if the sampling were carried out at the inlet to the HPT NGV, this is likely to be an impractical practice in an operating environment.

6. REFERENCES

[1] A. J. Wadcock, L. A. Ewing, and E. Solis, 'Rotorcraft Downwash Flow Field Study to Understand the Aerodynamics of Helicopter Brownout', in *Technologies for the Next Generation of Vertical Lift Aircraft*, Dallas-Fort Worth, 2008, p. 27.

[2] J. Milluzzo and J. G. Leishman, 'Assessment of Rotorcraft Brownout Severity in Terms of Rotor Design Parameters', *J. Am. Helicopter Soc.*, vol. 55, no. 3, pp. 32009–320099, Jul. 2010.

[3] C. Cowherd Jr, 'Sandblaster 2 Support of See-Through Technologies for Particulate Brownout', Midwest Research Institute, 2007.

[4] A. Hamed and W. Tabakoff, 'Erosion and Deposition in Turbomachinery', *J. Propuls. Power*, vol. 22, no. 2, pp. 350–360, Mar. 2006.

[5] J. E. Goodwin, W. Sage, and G. P. Tilly, 'Study of Erosion by Solid Particles', *Proc. Inst. Mech. Eng.*, vol. 184, no. 1, pp. 279–292, Jun. 1969.

[6] M. G. Dunn, 'Operation of gas turbine engines in an environment contaminated with volcanic ash', *J. Turbomach.*, vol. 134, no. 5, p. 051001, 2012.

[7] N. Bojdo, 'Rotorcraft Engine Air Particle Separation', University of Manchester, School of Mechanical Civil and Aerospace Engineering, 2012.

Presented at 45th European Rotorcraft Forum, Warsaw, Poland, 17-20 September, 2019

This work is licensed under the Creative Commons Attribution International License (CC BY). Copyright © 2019 by author(s).

[8] A. Kellersmann, S. Weiler, C. Bode, J. Friedrichs, G. Ramm, and J. Stading, 'Surface Roughness Impact on Low-Pressure Turbine Performance due to Operational Deterioration', p. 10, 2017.
[9] R. J. Clarkson and H. Simpson, 'Maximising Airspace Use During Volcanic Eruptions: Matching Engine Durability against Ash Cloud Occurrence', North Atlantic Treaty Organisation Science & Technology Organisation, MP-AVT-272-1, 2017.
[10] O. Sweetman, 'Hawaii V-22 Accident Investigation Points To New Ingestion Issue', *Aviation Week & Technology*, 2015. .
[11] N. Bojdo, M. Ellis, A. Filippone, M. Jones, and A. Pawley, 'Particle-Vane Interaction Probability in Gas Turbine Engines', *J. Turbomach.*, vol. 141, no. 9, p. 1, Jun. 2019.
[12] R. J. Clarkson, E. J. Majewicz, and P. Mack, 'A re-evaluation of the 2010 quantitative understanding of the effects volcanic ash has on gas turbine engines', *Proc. Inst. Mech. Eng. Part G J. Aerosp. Eng.*, vol. 230, no. 12, pp. 2274–2291, Oct. 2016.
[13] J. P. Bons, R. Prenter, and S. Whitaker, 'A Simple Physics-Based Model for Particle Rebound and Deposition in Turbomachinery', *J. Turbomach.*, vol. 139, no. 8, p. 081009, 2017.
[14] J. L. Smialek, F. A. Archer, and R. G. Garlick, 'Turbine airfoil degradation in the persian gulf war', *JOM*, vol. 46, no. 12, pp. 39–41, Dec. 1994.
[15] S. M. Whitaker and J. P. Bons, 'An Improved Particle Impact Model by Accounting for Rate of Strain and Stochastic Rebound', in *Volume 2D: Turbomachinery*, Oslo, Norway, 2018, p. V02DT47A016.
[16] C. A. Wood, 'Characterisation of Dirt, Dust and Volcanic Ash: A Study on the Potential for Gas Turbine Engine Degradation', Defence Science and Technology Group, 2017.

7. NOMENCLATURE

Roman Symbols

c	*Specific Heat Capacity*
h	*Vane Height*
k	*Thermal Conductivity*
m	*Mass*
m_f	*Mass Fraction*
$\dot{m}$	*Mass Flow Rate*
t	*Time*
$\boldsymbol{a}$	*Fitting Coefficient*
$\boldsymbol{b}$	*Fitting Coefficient*
$\boldsymbol{c}$	*Fitting Coefficient*
$\boldsymbol{d}$	*Fitting Coefficient*
B	*Yield Strength Reduction Coefficient*
C	*Concentration*
CoR	*Coefficient of Restitution*
D	*Disk Loading*
E	*Normal Kinetic Energy*
G	*Elastic Modulus*
M_{drag}	*Removal Drag Moment*
N	*Vane Number*
R^2	*Coefficient of Determination*
Re	*Reynolds Number*
Stk_{gen}	*Generalised Stokes Number*
Stk_{th}	*Thermal Stokes Number*
T	*Temperature*
U	*Velocity*
W_a	*Particle-Substrate Bond Strength*

Greek Symbols

γ	*Surface Free Energy*
δ	*Dose*
ζ	*Accumulation Factor*
μ	*Dynamic Viscosity*
ν	*Poisson Ratio*
ξ	*Retention Probability*
ρ	*Density*
σ_y	*Yield Strength*
ψ	*Non-Stokes Drag Correction Factor*
χ	*Interaction Probability*

Subscripts and Superscripts

$[.]_f$	*Pertaining to the fluid*
$[.]_p$	*Pertaining to the particle*
$[.]_{in}$	*Pertaining to the NGV inlet conditions*
$[.]_1$	*Pertaining to the particle before impact*
$[.]_{core}$	Pertaining to the core flow
$[.]_2$	*Pertaining to the particle after impact*
$[.]_n$	*Denotes normal to the vane surface*
$[.]_{NGV}$	*Pertaining to the Nozzle Guide Vane*
$[.]_{soft}$	Denotes particle softening conditions

Abbreviations

ARD	*Arizona Road Dust*
EAPS	*Engine-Air Particle Separator*
FOD	*Foreign Object Debris*
GE-E^3	*General Electric Energy Efficient Engine*
NGV	*Nozzle Guide Vane*
PSD	Particle Size Distribution

8. ACKNOWLEGEMENTS

Part of this work was joint funded by the UK Engineering and Physical Sciences Research Council (EPSRC) and the Defence Science and Technology Laboratory (DSTL), who are funding the doctoral studies of lead author, Matthew Ellis, as part of EPSRC grant EP/P510579/1.

Copyright Statement
The authors confirm that they, and/or their company or organization, hold copyright on all of the original material included in this paper. The authors also confirm that they have obtained permission, from the copyright holder of any third party material included in this paper, to publish it as part of their paper. The authors confirm that they give permission, or have obtained permission from the copyright holder of this paper, for the publication and distribution of this paper as part of the ERF proceedings or as individual offprints from the proceedings and for inclusion in a freely accessible web-based repository.

Presented at 45th European Rotorcraft Forum, Warsaw, Poland, 17-20 September, 2019
This work is licensed under the Creative Commons Attribution International License (CC BY). Copyright © 2019 by author(s).